Numerical and experimental investigation of sloshing phenomena in conditions of low filling ratios.

B.Bouscasse[1], A.Colagrossi[1,2], G.Colicchio[1,2], C.Lugni[1,2]

1. INSEAN, Italian Ship Model Basin, Rome
2. CESOS: Centre of Excellence for Ship and Ocean Structures, NTNU, Trondheim, Norway.

Introduction

A numerical model and experiments have been used to study some features of the flow developing in tanks forced to move with harmonic motion. Attention has been focused on the conditions of low filling ratios. In this cases, non-linearities are easily developed, and their features are strongly dependent on the following parameters: amplitude and frequency of oscillation and filling height. Here the parameter are chosen so to cause the occurrence of bore (according to [8]. Ondular bore and, critical cases, breaking bores will be shown. The modelling of these features requires a robust and accurate numerical solver, and the Smoothed Particle Hydrodynamics (SPH) has proved its ability to model them in the direct comparison with the experiments. In [6], the same solver has also shown the ability to model other, strongly non linear events as the dam-break flows, sloshing flows, ship flows and wave breaking process.

Experimental set up

A global sketch of the experimental setup is shown in left plot of figure 1: the tank is $L = 1$ m long, $b = 0.1$ m wide and is filled with water up to a height h. To ensure a purely sinusoidal motion $Asin(2\pi t/T)$ along the longitudinal direction, an *ad hoc* mechanical system has been used. Here A is the displacement amplitude and T is the period of the prescribed motion. The geometry of the tank, *i.e.* $b/L = 0.1$, ensures an almost-2D flow in the main tank plane.
Two capacitance wave probes are placed at the sides of the tank. The first one η_1 is positioned at a distance of 1 cm from one side, the second one η_2 at distance of 5 cm. During the tests, flow visualizations were performed through low- and high-speed digital video cameras. In particular, a low-speed camera (JAI CV-M2) with spatial resolution 1600x1200 pixels and frequency rate equal to 15 Hz was placed in front of the tank and sufficiently far from it to record the global behavior of the wave propagating. Further, a high-speed camera was placed closer to the front wall. Finally, a wire potentiometer was used for a direct measurement of the position of the tank. Particular care has been devoted to the synchronization of the several acquisition systems with different sampling rates, used for the recording of the signals. A suitable synchronizer has been used to trigger the start of the several acquisition systems at the selected time instants.

Numerical methods

Governing Field Equations The fluid evolution is governed by the Navier-Stokes equation in the domain Ω

$$\frac{\mathrm{D}\boldsymbol{u}}{\mathrm{D}t} = -\frac{\nabla p}{\rho} + \boldsymbol{f_v}(\boldsymbol{x},t) + \boldsymbol{f}(\boldsymbol{x},t) \tag{1}$$

where $\boldsymbol{f_v}(\boldsymbol{x},t)$ is the viscous force and $\boldsymbol{f}(\boldsymbol{x},t)$ are the external non inertial forces (see [3]).
Two strategies can then be adopted for the solution of the water domain. The first one is to consider the flow incompressible, implying that its velocity $\boldsymbol{u}$ is divergence free. Inserting this constraint into the Navier-Stokes equation leads to a Poisson equation for the pressure field p (this approach is usually used for the incompressible Navier-Stokes solvers). The second strategy (used in the SPH method) considers the flow as weakly-compressible, meaning that the pressure field is linked directly to the density field through an equation of state for example the equation $p = c_0^2(\rho - \rho_0)$ can be used. The weakly-compressible assumption implies that the speed of sound c_0 must be at least one order of magnitude greater than the maximum flow velocity.

CSPH (Corrected Smoothed Particles Hydrodynamic) The corrected Smoothed Particle Hydrodynamics (cSPH) mathematical model was developed into a join collaboration between INSEAN and Ecole Centrale de Nantes. The main details of the method are described in [3] and [4].

The basic idea is to consider a set of N particles distributed over the fluid domain Ω. Each particle is associated with a *kernel* (or *smoothing*) function W, and moves in the force field generated by the entire particles system. The mass conservation is intrinsically enforced since each particle has a constant mass all along the simulation. The SPH is a meshless method and all the variables are represented through interpolation integrals with suitable kernel functions W, (see *i.e.* [7] for a discussion of meshless methods). The essential features of the resulting algorithm are the complete absence of a computational grid and a fully Lagrangian character.

In discrete form $W_j(\boldsymbol{x}_i)$ indicates the kernel function centered on the particle j and evaluated in the generic point $\boldsymbol{x}_i$. In the following, the particle function $c_i = \sum_{k=1}^{N} W_k(\boldsymbol{x}_i)\, dV_k$ will be used; the summation is on the whole set of particle while dV_k indicates the volume of the generic particle k. Inserting the discrete formulation of the spatial derivatives, obtained through the integral interpolation, into the continuity and momentum equations, two systems of evolution equations for the ith particle are derived:

$$A)\begin{cases} \dfrac{\mathrm{D}ln\mathcal{J}_i}{\mathrm{D}t} = \displaystyle\sum_{j=1}^{N} \boldsymbol{u}_j \cdot \nabla W_j^{MLS}(\boldsymbol{x}_i)\, dV_j \\ \dfrac{\mathrm{D}\boldsymbol{u}_i}{\mathrm{D}t} = \displaystyle\sum_{j=1}^{N} p_j \nabla W_j^{MLS}(\boldsymbol{x}_i)\, dV_j + \\ \qquad\qquad \boldsymbol{f_v}(\boldsymbol{x}_i,t) + \boldsymbol{f}(\boldsymbol{x}_i,t) \end{cases} \qquad B)\begin{cases} \dfrac{\mathrm{D}ln\mathcal{J}_i}{\mathrm{D}t} = \displaystyle\sum_{j=1}^{N} (\boldsymbol{u}_j - \boldsymbol{u}_i) \cdot \nabla W_j(\boldsymbol{x}_i)/\, c_i\, dV_j \\ \dfrac{\mathrm{D}\boldsymbol{u}_i}{\mathrm{D}t} = \displaystyle\sum_{j=1}^{N} \left[\frac{p_j}{c_j} + \frac{p_i}{c_i}\right] \nabla W_j(\boldsymbol{x}_i)\, dV_j + \\ \qquad\qquad \boldsymbol{f_v}(\boldsymbol{x}_i,t) + \boldsymbol{f}(\boldsymbol{x}_i,t) \end{cases} \tag{2}$$

where $\mathcal{J}_i(t)$ is the ratio $dV_i(t)/dV_i(t=0)$ and W^{MLS} is the moving least square kernel defined in [7]. The set A of the evolution equations is used when the matrix which defines the W^{MLS} kernel is well-conditioned while the set B is used in the other cases (see [3]).

The evolution equations B are quite close to the standard SPH equations and present the same characteristics of robustness which are relevant to follow complex free surface dynamics. On the other hand the set of equation A permits a more accurate evaluation inside the bulk of the fluid, because of the MLS kernel.

Once $\mathcal{J}_i$ is evaluated, it is possible to calculate the volume distribution of the generic i-th particle: $dV_i(t) = \mathcal{J}_i\, dV_i(t=0)$. The density field is derived through the use of the MLS kernel:

$$\rho(\boldsymbol{x}_i) = \sum_j m_j\, W_j^{MLS}(\boldsymbol{x}_i)\, dV_j \tag{3}$$

where m_j is the mass of the generic j-th particle. The mass distribution has to be set in the beginning of the simulation, and the mass of each particle does not change during the time evolution. In equation (3), the MLS kernel is used only if the matrix, which defines this type of kernel, is well conditioned, otherwise the Shepard kernel W^S is adopted.

The free-surface boundary conditions are easily handled by the SPH method. More in detail, due to the Lagrangian character of the solver, the kinematic condition is intrinsically satisfied while the dynamic condition must be enforced as described in [4]. The solid boundaries are modeled through a 'ghost particles' technique. It consists in the local mirroring of the fluid with respect to the solid boundary for a length $3h$ inside the wall.

The viscous term $\boldsymbol{f_v}$ is modelled as described in [1], while the boundary layer effect is neglected because a free-slip condition is assumed on the tank walls.

The discrete divergence operator, on the right hand side of equations (2), has to be filtered in space at each time step. This permits to avoid unphysical high-frequency oscillations of the particle's volume, but causes numerical noise on the pressure field, and therefore on local loads on the tank wall. The numerical aspects of this correction are still under investigations.

The evolution equations can be stepped forward in time by any ODE integrator. In the present implementation a forth-order Runge Kutta is adopted with a dynamic choice of the time step

δt according to stability constraints.

Analysis

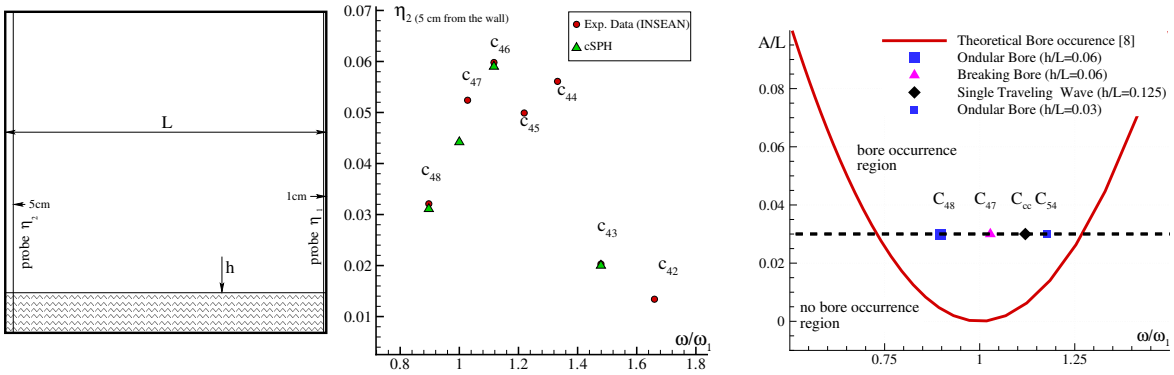

Figure 1: Left: sketch of the problem. Center: Maximum wave elevation for the sway excitation ($A = 0.03L$, $h = 0.06L$). Right: Occurrence diagram of bore type propagation.

case	h/L	ω/ω_1	case	h/L	ω/ω_1
C_{54}	0.030	1.178	C_{47}	0.060	1.028
C_{48}	0.060	0.897	C_{cc}	0.125	1.120

Table 1: Parameters of the analyzed test cases. For each case $A/L = 0.03$.

Identification of sloshing regimes This study is focused on the analysis of swaying tanks in conditions of filling ratios $h/L < 0.337$ and with frequency of oscillations in the range $[0.8, 1.8]\omega_1$, where ω_1 is the first natural sloshing period. These conditions imply that a *hard spring type* regime [5] realizes, that is the most energetic sloshing motions develop for frequencies of oscillation slightly higher than the natural frequency. Here, only $A = 0.03L$ will be analyzed.
The center plot in figure 1 shows the numerical and experimental average maximum wave height measured at $5cm$ from the wall (see left plot of the same figure). The behaviour corresponds to the one described in [5]. The circles in the plots correspond to the experimental data collected at INSEAN, while the triangles correspond to the numerical data obtained through the cSPH simulations. The labels shown in the plots are inherited from the experimental campaign and they will be used in the following to identify the different runs.
The range of frequency that will be analyzed in the following is wide and we aim to highlight the features of the flow developing. The response amplitude operator in figure 1 refers to an amplitude of oscillation $A = 0.03L$ and filling height $h = 0.06L$ (center plot). The maximum wave height doubles the initial water height. Once a critical frequency is overcome, say $\omega > 1.4\omega_1$, the amplitude of motion decays abruptly. The analysis of the experimental images and of the numerical simulations shows an almost linear behaviour of the free surface, *i.e.* it is the results of the superposition of sinusoidal standing waves.
The response operator shows that for $\omega/\omega_1 \in (0.8, 1.2)$ the strong non-linear effects take place. From the theory in [8] (see right plot of figure 1) indicates that, there, the waves always propagate in a bore form.

Propagation of ondular bores The left experimental pictures of figure 2 show the flow developing for the test C_{54} (see table 1). It is an ondular bore propagation. The comparison with the numerical solution left-bottom plot of figure 2 shows that the general behaviour is well captured. In cSPH simulation, the front of the bore breaks with a plunging jet with characteristic length of about 1cm. The surface tension (not modelled in the present numerical solver) prevents this phenomenon in experiments. Figure 3 shows the records of numerical

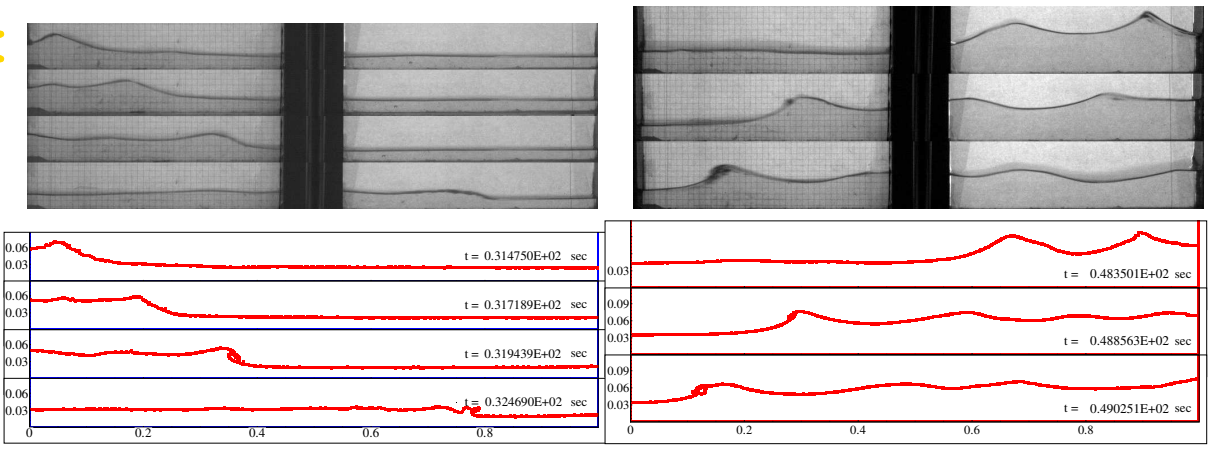

Figure 2: Experimental (top) and numerical (bottom) evolution of the free surface for the cases C_{54} (left) and C_{48} (right) (see table 1).

and experimental wave elevation at 5cm from the wall. The comparison is satisfactory, but for the maximum amplitude, which is higher in the numerical data, because of the breaking phenomenon. Moreover, the experimental data present successive local maxima related to the wave train following the bore front. They are hidden in the numerical solution by the presence of the breaking reflected by the wall and interacting with the following waves. This is more clearly visible in left plot of figure 4, where the contour plots of the numerical wave heights are plotted in the time-space plane. At $t/T = -0.2$ the breaking front is reflected by the wall and interacts with the two secondary waves. In this figure the celerity of the bore front is approximated by $\sqrt{gh}$ when it leaves the wall and increases to $2\sqrt{gh}$ before impacting the opposite side. Case

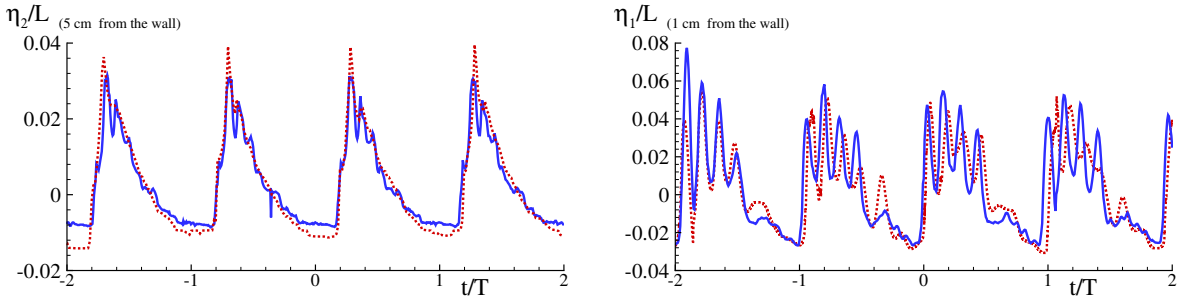

Figure 3: Wave height close to the wall for the cases C_{54} (left) and C_{48} (right) (see table 1. The solid line represents the experimental measurements, the dashed line stands for the numerical solution.

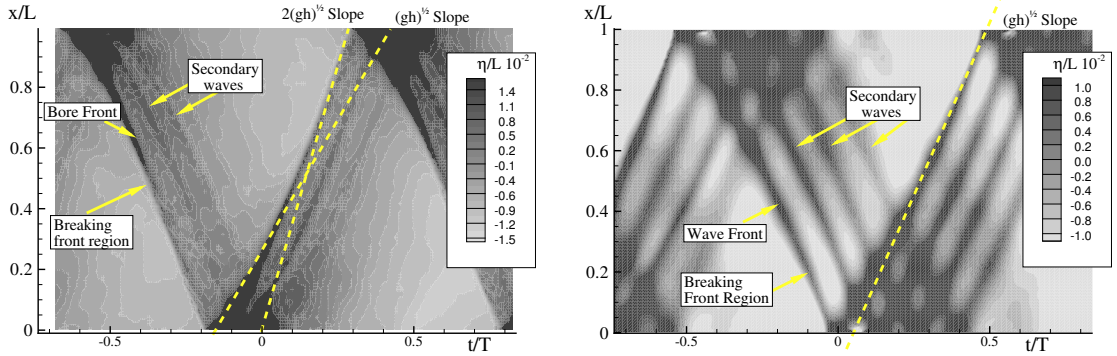

Figure 4: Evolution of the wave height in the cases C_{54} and C_{48} respectively from left to right.

C_{48} refers to a smaller excitation frequency, and double filling height. These parameters cause a more intense ondular bore with respect to the previous case. It is also characterized by a higher wave train and by a breaking stage realizing closer to the tank wall. The latter prevents

the development of a proper breaking front. These features are present both in the experiments and in the numerical simulations as shown by the right plots of figure 2. Such a similar good agreement is present in figure 3, where the wave heights η_1 (see figure 1 for definition) on the wall are compared. Both the tools of analysis show the presence of four peak of the η_1 time record. They are due to the presence of three waves following the bore front in the wave train as made evident in the right of figure 4. The same plot shows that the bore front travels with a celerity close to $\sqrt{gh}$.

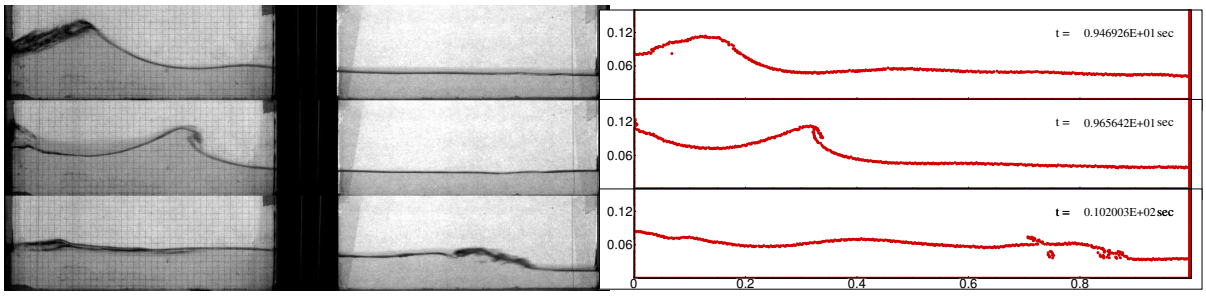

Figure 5: Experimental (left) and numerical (right) evolution of the free surface for the case C_{47} (see table 1).

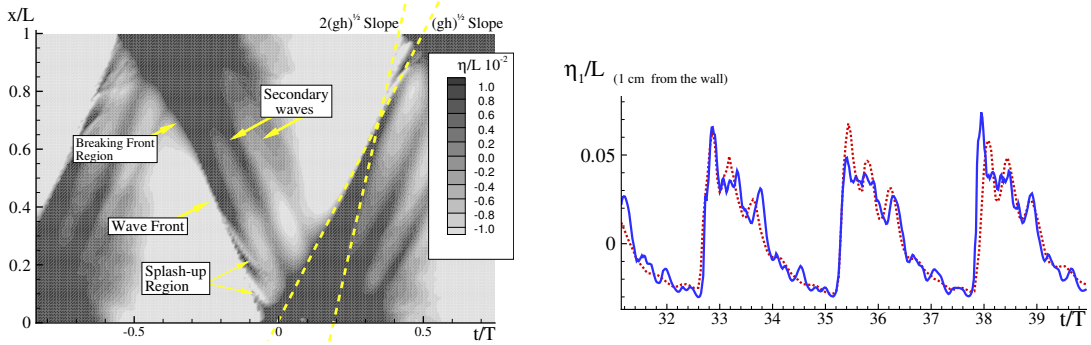

Figure 6: Evolution of the wave height in time-space plane (left) and wave height close to the wall versus time (right) for the case C_{47}

Propagation of breaking bores In the previous paragraphs, the evolution of the free surface has been analyzed for frequencies both in the higher and lower neighbourhood of the first natural one. In the test case C_{47} (see table 1 the ratio $\omega/\omega_1 \simeq 1$ and, as show for the case C_{54}, the free surface is characterized by the presence of an ondular bore (see figure 5). Differently from what noticed before, here both the numerical data and the experimental images present a breaking front already developing before the mid of the tank. This means that a breaking bore develops. Its trace is highlighted on the time-space plane of figure 6. The same figure shows the presence of two secondary waves as in case C_{54}, confirmed by the three peaks of the wave height, recorded close to the wall (right side of figure 6). Another feature of the breaking bore is the presence of the splash-up region, whose trace are visible in the time-space plane, when the bore front approaches the opposite wall. When the splash-up appears, the bore front changes its celerity from $\sqrt{gh}$ to $2\sqrt{gh}$.

Sloshing steep wave impacting against walls Further increasing the filling ratio up to 0.125, while ω is slightly higher than the natural frequency ω_1, the ondular bore disappears for a single wave-front that moves with a celerity $2\sqrt{gh}$. When approaching the opposite wall, it becomes very steep and, eventually, breaks against the wall. This is the critical condition studied in [3], because of the violent and localized impacts on the tank wall. Left figure 7 shows the evolution of the free-surface up to the impact, while the right side gives the wave evolution on the time-space plane. Here the propagation of the wave front is highlighted as well as the effect of the impact on the wall. This one causes a high run-up, whose maximum value is reached

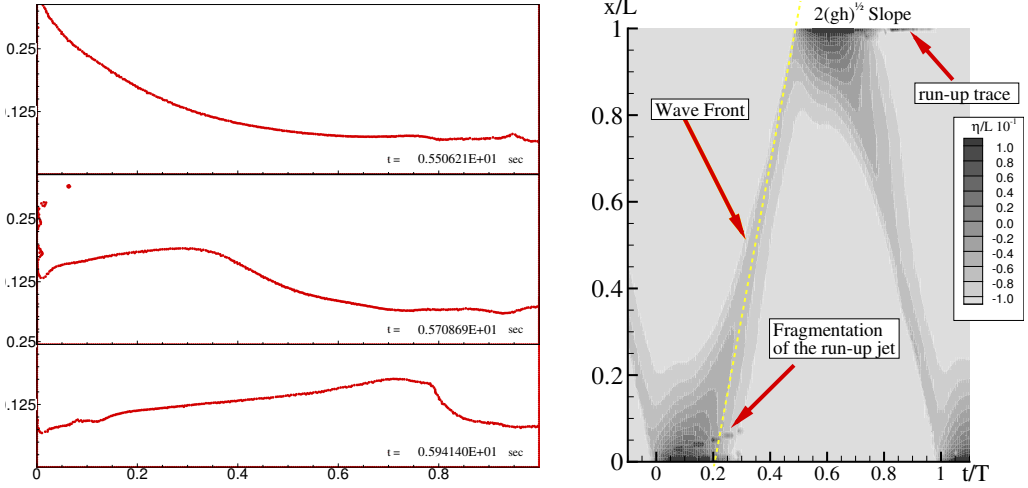

Figure 7: Numerical evolution of the free surface (left) and evolution of the wave height in time-space plane (right) for the case $A = 0.03L$, $h = 0.125L$, $\omega/\omega_1 \simeq 1.12$.

in about 1/6 of the excitation period. At that time the wave starts to propagate in the other direction, while the gravity collapse takes another 1/6 of excitation period.

Acknowledgements
The present research activity is partially supported by *CESOS: Centre of excellence for Ship and Ocean Structures, NTNU, Trondheim, Norway*, within the project, *S̈loshing flows¨* and partially by *Ministero dei Trasporti* within the *P̈rogramma di Ricerca 2007-2009¨*.

References

[1] Monaghan, J.J. 2005 Smoothed Particle Hydrodynamics. *Reports on Progress in Physics.* Institute of Physics Publishing, **68**, 1703-1759.

[2] Colagrossi, A., & Landrini, M. 2003 Numerical simulation of interfacial flows by Smoothed Particle Hydrodynamics. *Journal of Computational Physics.* **191**, 448-475.

[3] Colicchio, G., Colagrossi, A., Lugni, C., Brocchini, M. & Faltinsen O.M. 2007 Challenges in the numerical investigation of the flip-through *Proc. 9th Int. Conf. in numer. ship hydr., Michigan.* **2**, 95-104.

[4] Landrini, M., Colagrossi, A., Greco, M. & Tulin, M.P. 2007 Gridless simulations of splashing processes and near-shore bore propagation *to be published on Journal of Fluid Mechanics.*

[5] Faltinsen, O.M. & Rognebakke, O.F. 2000 Sloshing. *Proc. Int. Conf. on Ship and Shipping Research.* Venezia, Italy.

[6] Colagrossi, A. 2005 Meshless Lagrangian Method for Free–Surface and Interface Flows with Fragmentation, *PhD Thesis University of Rome,* La Sapienza *Italy (http://padis.uniroma1.it)*

[7] Fries, T.P. & Matthies, H.G. 2004 Classification and Overview of Meshfree Methods. *Informatikbericht 2003-03, Institute of Scientific Computing, Technical University Braunschweig, Brunswick, Germany.*

[8] Verhagen, J.H.G. & Van Wijngaarden,L. 1965 Non linear oscillation of fluid in a container. *J. of Fluid Mechanics* **22**.